Glass Europe Vol. 3 (2025) 253-264

https://doi.org/10.52825/glass-europe.v3i.2575

Submitted: 01 Jul. 2025 | Accepted: 04 Aug. 2025 | Published: 08 Jan. 2026

Optical, Structural, and Electrical Properties of TeO_2 – Na_2O – NaX Glasses (X = Cl, Br, I): Roles of Crucible Materials and Halides

Xuanzhao Pan[1,2], Jiangbo Zhao[1,3], Bruno Poletto Rodrigues[1,4,5], Alexis Duval[4], Lothar Wondraczek[4,6,*], and Heike Ebendorff-Heidepriem[1,2]

[1]Institute for Photonics and Advanced Sensing, and School of Physics, Chemistry and Earth Sciences, The University of Adelaide, Adelaide, SA, Australia

[2]Centre for Nanoscale BioPhotonics, University of Adelaide, Adelaide, SA, Australia

[3]School of Engineering, Faculty of Science and Engineering, University of Hull, Cottingham Rd, Hull HU6 7RX, United Kingdom

[4]Otto Schott Institute of Materials Research, Friedrich Schiller University Jena, Fraunhoferstraße 6, 07743 Jena, Germany

[5]Fraunhofer Institute for Applied Optics and Precision Engineering, Albert-EinsteinStraße 7, 07745 Jena, Germany

[6]Center for Energy and Environmental Chemistry – CEEC, Friedrich Schiller University Jena, Philosophenweg 7, 07743 Jena, Germany

[*]Correspondence: Lothar Wondraczek, lothar.wondraczek@uni-jena.de

Abstract. Alkali tellurite glasses, which offer a broad glass-forming region along with large halide solubility, are excellent candidates as transparent conductive materials. TeO_2 – Na_2O – NaX (X = Cl, Br, I) glasses with halogen contents X ranging from 0 to 6 at. % (in total at. % of constituting elements Te, Na, O, and X) are investigated. Au crucibles alter their optical properties through the formation of inhomogeneously distributed gold nanoparticles. In contrast, alumina crucibles, despite undergoing a more severe dissolution, result in minor changes of the glasses' structural and electrical properties. The electrical conductivity of such mixed anion glasses hinges on the mobility of the charge carriers (Na^+ ions), and thus (i) on the bond strength of the Na-X bonds involved, as well as (ii) on the free volume within the glass network and consequently on the size of the anions. Accordingly, the electrical conductivity is found independent on the substitution rate for small halogens (X = Cl, Br), but increases up to three-fold for large halogens (X = I).

Keywords: Tellurite Glasses, Oxyhalides, Structure, Electrical Conductivity, Optical Properties

1. Introduction

TeO_2-based glasses offer a unique combination of properties, including visible to infrared range transmission, high refractive index, low melting temperature, and high rare-earth solubility. They find numerous uses in optics and photonics technologies, notably as optical waveguide amplifiers as well as in laser applications [1], [2], [3], [4]. Nonetheless, few efforts were devoted in exploiting their excellent transparency for the design and development of transparent conductive materials. Indeed, achieving transparency in the visible range with millimeter

thickness is particularly challenging for conductive materials [5], [6], [7], [8], owing to the intertwined competing mechanisms of electronic conduction and transparency [9].

Ionic conductive glasses, and more particularly oxyhalide glasses, show promises in this regard. The electrical conductivity of halogen-containing SiO_2-, B_2O_3-, and P_2O_5-based glasses – chiefly driven by the mobility of the constituting alkali ions, *i.e.*, ionic conductivity – were extensively studied [10], [11], [12], [13], [14], [15], [16], revealing that the substitution of oxygen for halogens results in a substantial increase of their electrical conductivity. Despite the limited attention given to TeO_2-based oxyhalide glasses, they show comparable increases in electrical conductivity notably in the TeO_2 – Li_2O – LiCl ternary system [17], which calls for further exploration.

The present study thus focuses on TeO_2 – Na_2O – NaX (X = Cl, Br, or I) oxyhalide glasses. Indeed, the glass-forming region in the TeO_2 – Na_2O binary system extends up to 32 mol. % in Na_2O, which offers a large concentration of mobile charge carriers. In addition, tellurite melts demonstrate a high halide solubility [10]. The emphasis is therefore placed on the distinct roles of (i) halogen concentration and type (by increasing the substitution rate X/[O+X] while preserving the initial Na to Te cationic ratio) and (ii) crucible materials, both of which are of paramount importance on the glasses' macroscopic properties, especially given the highly corrosive nature of TeO_2-based melts [18], [19].

2. Materials and methods

2.1 Sample preparation

Three series of glasses with nominal compositions $(TeO_2)_{0.68}[(Na_2O)_{0.32-x/2}(NaX)_x]$ were prepared via the melt-quenching method, with X = Cl, Br, or I. These compositions were defined so as to maintain a fixed Na to Te cationic ratio, with the halogen concentration as the sole variable. Values of *x* were varied so as to reach substitution rates (X/[O+X]) ranging from 0 to 16 %. The samples were labeled TN-X-SR, where SR stands for substitution rate. Glass batches were prepared from analytical grade raw materials, stored in a N_2-purged glovebox: TeO_2 (99.999 %, CNBM, optoelectronic materials, Chengdu, China), Na_2CO_3 (99.5 %, Chem-Supply), NaCl (99.7 %, Chem-Supply), NaBr (99 %, General-Purpose-Reagent), and NaI (99.5 %, Chem-Supply). Appropriate quantities of each reactant were weighed in a N_2-purged glovebox to avoid moisture absorption, and thoroughly mixed to ensure proper homogeneity. The mixed starting materials were then transferred either in alumina or gold crucibles, and subsequently heated in a box furnace in ambient atmosphere to 450 °C with a 20 $K \cdot min^{-1}$ heating rate for 2 h to facilitate the CO_2 release from Na_2CO_3 decomposition [20]. The crucibles were then covered respectively with platinum or gold lids, and heated to 750 °C with a 10 $K \cdot min^{-1}$ heating rate for 0.5 h. The melts were finally cast into brass molds, annealed 40 °C below their respective glass transition temperatures for 2 h [21], and cooled down to room temperature with a 0.1 $K \cdot min^{-1}$ cooling rate. The procedure slightly differed in the case of the two most iodine-rich glasses: the iodine-free melt was first cast, the obtained glass was grounded into a fine powder, mixed with the adequate amount of NaI, and remelted at 600 °C for an additional 0.5 h before final quenching and annealing. The specimens, typically 40 g large, were polished to optical-grade quality and stored in a desiccator until further characterization.

2.2 Characterization

The halogen contents X were determined using a Cameca SX-Five electron probe microanalyzer (EPMA), equipped with five tunable wavelength-dispersive spectrometers. The instrument was operating at 20 nA and 15 kV, with a 20 µm defocused beam.

Elemental compositions (± 1 at. %, in total at. % of constituting elements Te, Na, O, and X) were analyzed utilizing a FEI Quanta 450 FEG environmental scanning electron microscope (SEM), equipped with an energy-dispersive X-ray spectroscope (EDX).

X-ray diffraction (XRD) profiles were collected using a Rigaku MiniFlex 600 diffractometer with Cu-K_α radiation (1.5418 Å), a scan speed of 3°·min^{-1}, and a step size of 0.02°. The working current and voltage of the X-ray tube were 15 mA and 40 kV, respectively.

The ultraviolet-visible (UV-Vis) absorbance spectra were acquired using a UV-Vis spectrophotometer (Cary 5000, Agilent Technologies), with a scan speed of 600 nm·min^{-1}, and a 1 nm resolution.

The density of each specimen was determined by the Archimedes method at 25 °C utilizing 1,2-propanediol as the solvent (ρ = 1.036 g·cm^{-3}).

Differential scanning calorimetry coupled with thermogravimetric analysis (DSC-TGA) experiments were conducted using a TGA/DSC 2 thermogravimetric analyzer (Mettler Toledo). Each sample was loaded in a platinum crucible, and gradually heated with a 20 K·min^{-1} heating rate under nitrogen flow.

The Raman spectra were obtained with a Renishaw inVia Raman microscope equipped with a 2400 lines/mm diffraction grating, using a 514.5 nm excitation wavelength (Ar-ion laser beam) with a 0.1 mW·µm^2 power density. The resolution was 2 cm^{-1}.

The impedance spectra of gold-sputtered glass specimens were measured with a Novocontrol Alpha-A impedance spectrometer and a Novotherm temperature control system. Electrical conductivity (σ_{DC}) was assessed over the 10^{-1} – 10^7 Hz frequency range and 80 – 170 °C temperature range (in 30 °C steps), by deriving the resistance under direct current (R_{DC}) from Nyquist plots, following:

$$\sigma_{\mathrm{DC}} = \frac{1}{R_{DC}} \cdot \frac{l}{A} \tag{1}$$

where l and A are the thickness and the area of the sample, respectively. The temperature dependence of the electrical conductivity was described using an Arrhenius-type equation, from which the activation energy for electrical conductivity (E_a) was extracted according to:

$$\sigma(T) = \frac{\sigma_0}{T} exp\left(-\frac{E_a}{k_B T}\right) \tag{2}$$

where σ_0 is a pre-exponential factor, T is the temperature, and k_B is the Boltzmann constant.

3. Results and discussion

3.1 Sample characterization

Weight losses during the oxyhalide glass syntheses were only observed when X = I. These were evidenced in the form of purple vapors escaping from the melt, characteristic of gaseous I_2, and further confirmed through EPMA analyses. The quantified substitution rates were typically 40 % smaller with respect to the nominal compositions. Indeed, iodides (here NaI) are oxidized notably by atmospheric oxygen, following [22]:

$$4\ NaI + O_2 \rightarrow 2\ Na_2O + 2\ I_2 \tag{3}$$

The synthesis procedure was thus adapted for the two most iodine-rich glasses. Sodium iodide was added to a pre-synthesized iodine-free glass to minimize high-temperature exposure. The subsequent remelting of this mixture was then performed at lower temperatures, so as to limit the thermally activated reaction (3), while ensuring the melt remained sufficiently fluid for adequate homogenization and quenching. This approach effectively limited iodine loss, resulting in substitution rates that were but 10 % smaller than the nominal values.

The XRD patterns of the most halogen-rich glass samples are presented in Figure 1(a). The absence of distinct diffraction peaks and the presence of several broad humps in the 10 – 60° 2θ range confirm their amorphous nature, and hence the substitution of oxygen for halogens. This is indicative that, for substitution rates of oxygen by halogen of the order of 7 % for Cl and 10 – 11 % for Br and I, halides are successfully dissolved in the melts. The anion size seemingly plays a major role in the glass forming ability of oxyhalide melts, where larger halogens (X = Br, I) allow to increase the maximum substitution rate by approximately 40 % with respect to small halogen (X = Cl). For larger substitution rates, the excess halides recrystallize, and additional crystals of paratellurite (α-TeO_2), as well as Na_2TeO_3 when X = I, are formed.

UV-vis absorbance spectra and photographs of TN-Cl-SR glass samples with increasing substitution rates and varying crucible materials are shown in Figure 1(b). All glasses are transparent in the visible domain; however, glasses produced in Au crucibles exhibit a diffused yellow tint, while those synthesized in Al_2O_3 crucibles are colorless. This hue is attributed to the presence of gold ions and nanoparticles originating from the Au crucible corrosion [23]. Specifically, when the melt cools down during casting, it goes through the critical temperature range of 500-600 °C for gold nanoparticle formation. As evidenced by absorption bands located in the 500 – 700 nm region, the size of these metallic particles is particularly small (< 20 nm inferred from data in [23]), which coincides with the melt being only for a few seconds within the critical temperature range for gold nanoparticle formation. This short time also explains their non-uniform distribution in the final glasses. The gold contamination is typically of the order of 10 ppm [18], [23], [24], while that of alumina was quantified at 4 mol. %, irrespective of the halide content. Due to the incorporation of the lighter alumina into the tellurite network, the UV absorption edge is redshifted from 3.6 to 3.5 eV. Interestingly, the UV absorption edge is seemingly independent on the substitution rate, and no clear correlation with the absorption coefficient was identified. Hence, while the contamination of the tellurite glasses by Au crucibles induces imperceptible changes of their composition and thus of their macroscopic properties with respect to Al_2O_3 crucibles, the introduction of gold nanoparticles may pose a risk in the view of applications requiring precisely defined optical properties.

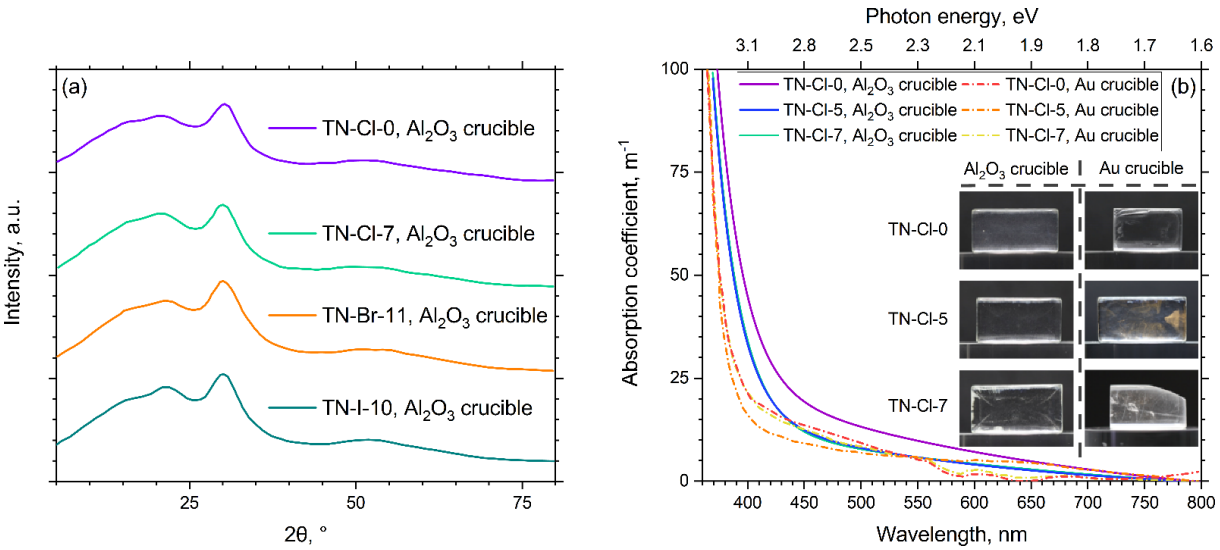

Figure 1. *(a) XRD patterns of TN-X-SR glasses synthesized in Al_2O_3 crucibles. (b) UV-Vis absorbance spectra of TN-Cl-SR glasses with increasing halogen contents and varying crucible materials. The inset presents photographs of 2 to 3 cm wide specimens.*

The density (ρ) and the glass transition temperature (T_g) of the investigated glasses are only slightly dependent on the halogen types and contents and the crucible materials. They respectively stand at values of 4.32 g·cm^{-3} and 241 °C for the halogen-free glass, and they decrease at most by 0.05 g·cm^{-3} and 5 °C in the most halogen-rich samples. Substituting Al_2O_3 crucibles for Au crucibles induces oppositely an increase in density of 0.04 g·cm^{-3}, and a decrease in glass transition temperature of 8 °C.

The molar volume (V_m), the packing density (C_g), and the free volume (V_{free}) of the various glass samples are calculated from the corresponding glass composition and density, following [25], [26]:

$$V_m = \sum \frac{f_i M_i}{\rho} \tag{4}$$

$$C_g = \frac{N_A \sum \frac{4}{3}\pi f_i {r_i}^3}{V_m} \tag{5}$$

$$V_{free} = V_m - N_A \sum \frac{4}{3}\pi f_i {r_i}^3 \tag{6}$$

where f_i and M_i are respectively the atomic fraction and the molar mass of the ith constituting element, r_i is its corresponding ionic radius, and N_A is the Avogadro number. The packing density serves as a measure of the atomic packing efficiency in a given matrix, and is thus reflective of the structural arrangements of its building blocks, while the free volume indicates the volume unoccupied by the ions. On the one hand, the packing density linearly increases by about 10 % of its original value when the substitution rate reaches approximately 10 %, with the effect being more pronounced as the ionic radius of the halogen increases (see Figure 2(a)). On the other hand, the free volume shows different trends (shown in Figure 2(b)). Where for small halogens (X = Cl, Br) the free volume decreases as the substitution rate increases, it oppositely increases for the large halogen (X = I). The consistent trend in packing density for all halogens is indicative of similar reorganizations of the glass network as halogens substitute for oxygen, specifically in the short- to medium-range order. The different trends in free volume are attributed to the different sizes of the halogens.

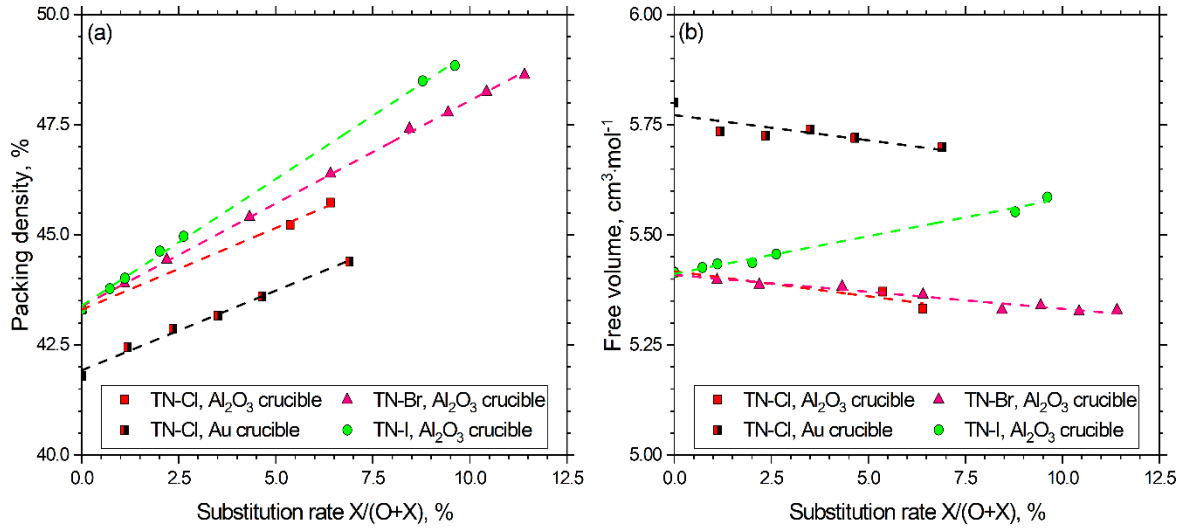

Figure 2. *(a) Packing density, and (b) free volume of TN-X-SR glasses with increasing halogen contents and varying crucible materials.*

3.2 Raman spectroscopy

Table 1*. Summary of the vibrational modes in sodium tellurite glasses observed by Raman spectroscopy.*

Peak	Position (cm^{-1})	Assignment
A	~ 775	Stretching vibration of Te-NBO_A bonds, where NBO_A does not interact with adjacent Te-based polyhedra
B	~ 725	Stretching vibration of Te-NBO_B, where NBO_B interacts with adjacent Te-based polyhedra
C	~ 670	Vibrations of inequivalent Te-O-Te linkages
D	~ 610	Stretching of [TeO_4] polyhedra
E	~ 470	Symmetric bending and stretching vibrations of Te-O-Te linkages of [TeO_N] polyhedra (N = 4, 3+1, and 3)
F	~ 275	Bending vibrations of Te-NBO in [TeO_3] polyhedra
G	~ 130	Intra-molecular asymmetric motions of Te-O bonds
Boson	~ 40	Localized vibrational modes; signature of structural disorder in the medium- to long-range length scale

A typical Raman spectrum of a sodium tellurite glass is depicted in Figure 3(a). The vibrational modes were identified following previous investigations performed on various TeO_2 – Na_2O glasses [27], [28], [29], [30], [31], [32], [33], [34], [35], [36], [37], [38], [39], [40]. They are schemed in Figure 3(a), and subsequently described in Table 1. Briefly, peaks A, B, and F are associated with vibrational modes involving Te-NBO (non-bridging oxygens) bonds, whereas peaks C and E involve the vibrations of Te-O-Te linkages. The compositional dependence of their areas, which can be used as an ersatz of the concentration of the corresponding bonds, is shown in Figure 3(b) and Figure (c) respectively. The area of vibrational modes involving Te-NBO bonds linearly decreases as the substitution rates increase, whereby the slope of decrease becomes higher with increasing halogen size. For a constant cationic composition, the substitution of 2-fold oxygen atoms for 1-fold halogen atoms results in a decrease in the concentration of anions, and consequently of NBO. In contrast to the NBO decrease, the area of vibrational modes involving Te-O-Te linkages increases, with the slope also being larger for the larger halogens. This strongly suggests that halogens preferentially substitute NBO over BO (bridging oxygens), which in turn promotes the formation of Te-O-Te linkages. This is supported by a gradual shift of the position of vibrational modes involving Te-NBO bonds towards larger wavenumbers, reflecting a change in their local environment, whereas the position of

vibrational modes involving Te-O-Te linkages remain unaltered, indicating that their local environment does not change (see Figure (d) and Figure (e), respectively). In other words, halogens preferentially form bonds with network modifier (Na-X) rather than with network formers (Te-X).

The trends observed with increasing substitution rates are only slightly affected by the use of Al_2O_3 crucibles. As Au crucibles are substituted for Al_2O_3 crucibles, the concentration of Te-NBO bonds increases, while that of Te-O-Te linkages decreases. Furthermore, the position of vibrational modes involving Te-O-Te linkages is blue-shifted. This is a clear indicator that [AlO_N] polyhedra (N = 4, 5, and 6) are incorporated in the tellurite glass network, through the formation of Te-O-Al linkages at the expense of Te-O-Te linkages [41], [42], [43], [44].

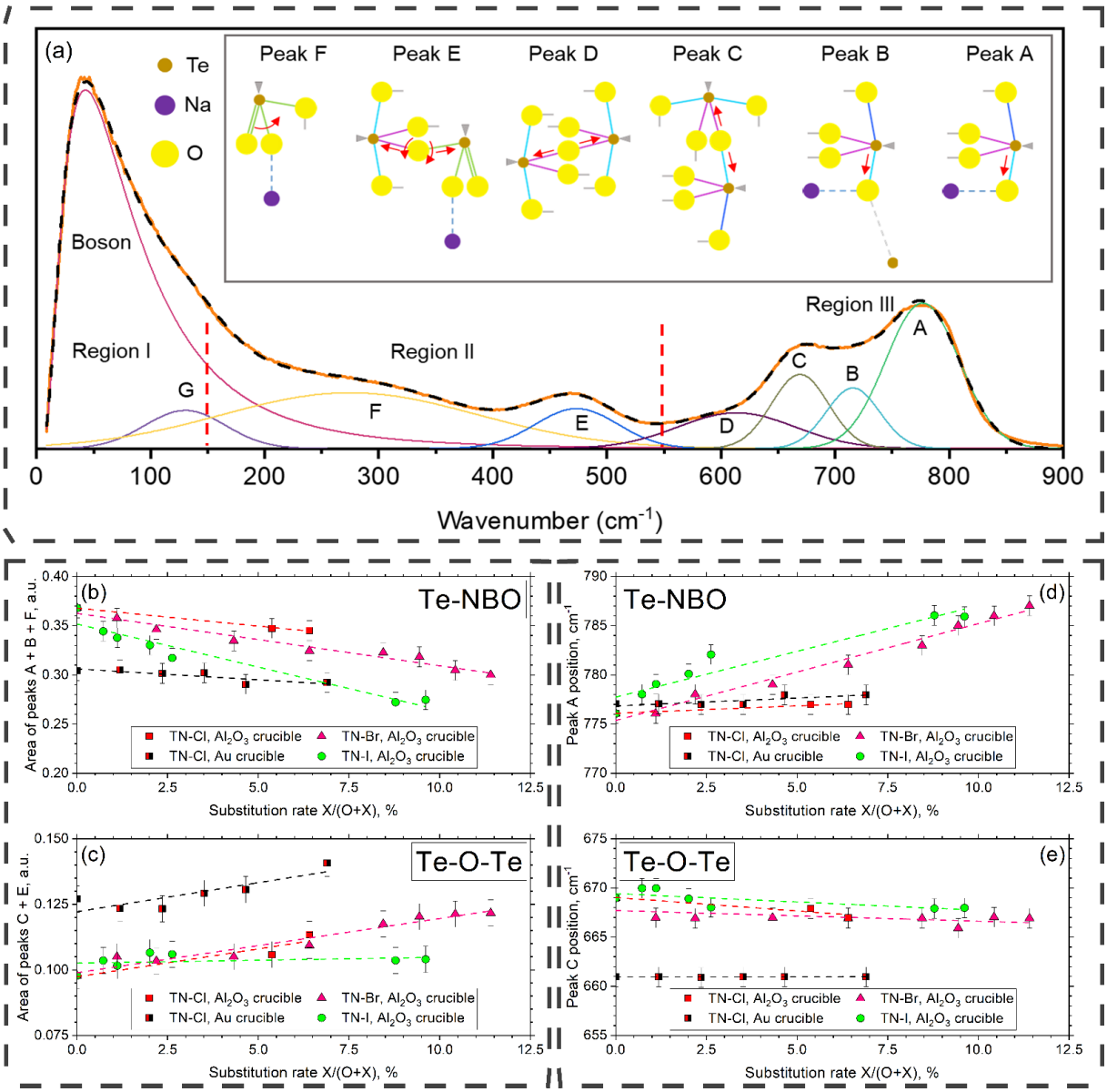

Figure 3. *(a) Typical Raman spectrum of a sodium tellurite glass. The vibrational modes attributed to each peak are shown schematically. Dependence on the halogen contents and crucible materials of the area of peaks ascribed to (b) Te-NBO vibrational modes (peaks A, B, and F), and (c) Te-O-Te vibrational modes (peaks C and E). Dependence on the halogen contents and crucible materials of the peak position of (d) Te-NBO vibrational modes (peak A), and (e) Te-O-Te vibrational modes (peak C).*

3.3 Electrical conductivity

The electrical conductivity of the various glass specimens is represented in Figure (a). For the smaller halogens X = Cl or Br, the electrical conductivity is seemingly independent on the substitution rate and crucible materials, standing at nearly constant values of $10^{-10.5}$ and $10^{-7.8}$ S·cm^{-1} at 80 and 170 °C, respectively. In contrast, for the larger halogen X = I, the electrical conductivity surprisingly triples as the substitution rate reaches approximately 10 %. Yet, the activation energy for electrical conductivity is very similar from one glass to another, as all values are comprised in the 0.95 ± 0.10 eV interval (see Figure (b)). This strongly suggests similar charge conduction mechanisms across the studied glass specimens.

The electrical conductivity in sodium tellurite glasses is governed by both the mobility and concentration of mobile charge carriers, i.e., here Na+ cations. In this work, the cation concentrations were kept constant across the various glasses. Hence, the halogen dependence of the electrical conductivity is unambiguously intertwined with the charge carrier mobility. It can be better understood by considering both the nature of the Na-X bonds as well as the compositional dependence of the free volume. On the one hand, halogens are more polarizable than oxygen, and exhibit increasingly smaller field strengths F ($F = z/r^2$), where z and r are the valence and the ionic radius of a given ion, respectively) from chlorine to iodine. In addition, Cl–, Br–, and I– form increasingly weaker bonds with Na+ (410, 370, and 301 kJ·mol-1, respectively). This results in more loosely bounded constituents and finally in an increased mobility of Na+ ions [10], [45], [46]. On the other hand, the mobility of cations is dictated by the dimensionality of the matrix, as well as by the volume available for ion movement, i.e., by the free volume. Indeed, while the glass network becomes more efficiently packed as the halogen's ionic radius increases, the free volume first decreases when X = Cl or Br, and subsequently increases when X = I. These two distinct and competing mechanisms therefore enable to describe the observed changes in electrical conductivity. For small halogens, the decrease in free volume counteracts the decrease in bond strength, so that the effective mobility of Na+ ions and thus the glass electrical conductivity remain unchanged. However, large halogens inversely induce an increase in free volume which, in tandem with the less tightly bounded Na+ ions, result in an increase of the charge carrier mobility and in fine in an increased electrical conductivity.

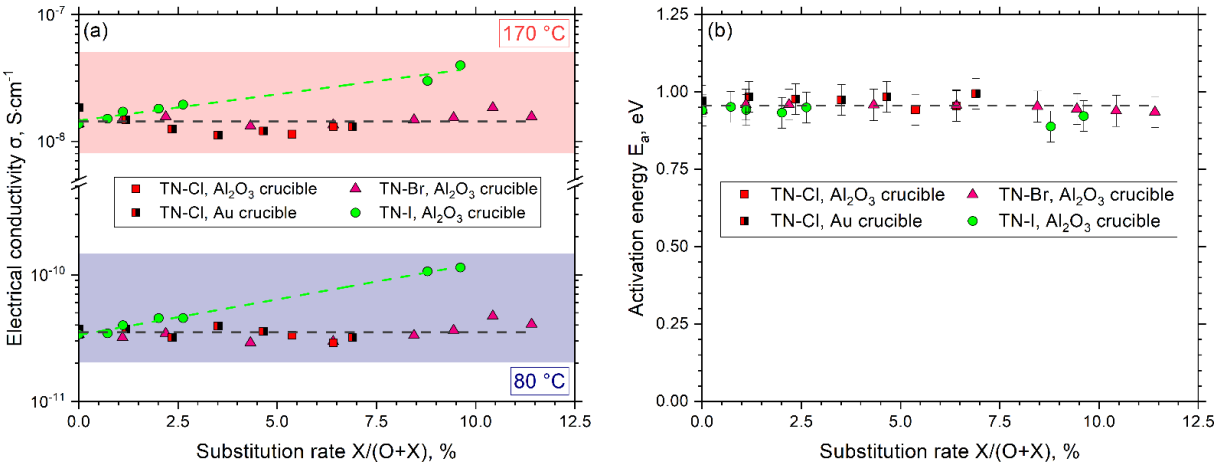

Figure 4. *(a) Electrical conductivity at 80 and 170 °C, and (b) activation energy for electrical conductivity of TN-X-SR glasses with increasing halogen contents and varying crucible materials.*

4. Conclusion

Sodium tellurite oxyhalide glasses (X = Cl, Br, or I) with substitution rates of oxygen for halogens up to 11 % were successfully obtained. Au crucibles dissolved to a small extent, leading to the formation of small gold nanoparticles dispersed inhomogeneously in the final glasses,

whereas inclusions-free glasses with approximately 4 mol. % of dissolved Al_2O_3 were produced when using alumina crucibles. The choice of crucible materials thus notably affects the glasses' optical properties, albeit with minor consequences on their structural and macroscopic properties.

Chlorine, bromine, and iodine all induced similar structural rearrangements of the glass network. They preferentially substitute non-bridging oxygens, which in turn favors inter-polyhedral linkages. The increase in packing density and the halogen dependence of the free volume directly hinges on the halogen's ionic radius. Each oxyhalide glass share similar charge conduction mechanisms, but they demonstrate different dependence of the electrical conductivity on the substitution rate. As the halogen's ionic radius increases, the Na-X bond strength decreases, whereas the free volume first decreases and then increases. Consequently, the Na^+ ions mobility and thus the glasses' electrical conductivity remain constant irrespective of the halogen substitution rate for small halogens (X = Cl, Br), but contrastingly increase remarkably for large halogens (X = I). In essence, the choice of the halogen is as important as the substitution rate for effectively controlling and designing the glasses' electrical properties.

Data availability statement

The data that support the findings of this study are available from the corresponding author upon reasonable request.

Author contributions

XP: Writing – Original Draft, Investigation. **JZ:** Validation, Investigation. **BPR:** Writing – Review & Editing, Validation, Investigation. **AD:** Writing – Review & Editing, Validation, Investigation. **LW:** Writing – Review & Editing, Supervision, Conceptualization. **HEH:** Writing – Review & Editing, Supervision, Conceptualization.

Competing interests

The authors declare that they have no competing interests.

Funding

We acknowledge financial support from the Carl Zeiss Foundation through its Breakthrough program (2018), and from the Australian Research Council grants CE140100003 and DP170104367. This work utilized the facilities at the Australian National Fabrication Facility (ANFF) OptoFab node funded by Australian Commonwealth and South Australian State Government.

References

[1] Y. Mizuno, M. Ikeda, and A. Yoshida, "Application of tellurite bonding glasses to magnetic heads," *J. Mater. Sci. Lett.,* vol. 11, no. 24, pp. 1653-1656, 1992, doi: 10.1007/BF00736198.

[2] R. El-Mallawany and M. Sayyed, "Comparative shielding properties of some tellurite glasses: Part 1," *Phys. Rev. B Condens.,* vol. 539, pp. 133-140, 2018, doi: 10.1016/j.physb.2017.05.021.

[3] H. Cankaya and A. Sennaroglu, "Bulk Nd3+-doped tellurite glass laser at 1.37 μm," *Appl. Phys. B,* vol. 99, no. 1, pp. 121-125, 2010, doi: 10.1007/s00340-009-3752-0.

[4] I. V. Kityk *et al.*, "Er–Pr doped tellurite glass nanocomposites for white light emitting diodes," *Opt. Commun.,* vol. 285, no. 5, pp. 655-658, 2012, doi: 10.1016/j.optcom.2011.10.088.
[5] T. Arai, "The study of the optical properties of conducting tin oxide films and their interpretation in terms of a tentative band scheme," *J. Phys. Soc. Jpn.,* vol. 15, no. 5, pp. 916-927, 1960, doi: 10.1143/JPSJ.15.916.
[6] Y. Zhao, G. A. Meek, B. G. Levine, and R. R. Lunt, "Near-infrared harvesting transparent luminescent solar concentrators," *Adv. Opt. Mater.,* vol. 2, no. 7, pp. 606-611, 2014, doi: 10.1002/adom.201400103.
[7] D. J. Lipomi *et al.*, "Skin-like pressure and strain sensors based on transparent elastic films of carbon nanotubes," *Nat. Nanotechnol.,* vol. 6, no. 12, pp. 788-792, 2011, doi: 10.1038/nnano.2011.184.
[8] Y. LeChasseur *et al.*, "A microprobe for parallel optical and electrical recordings from single neurons in vivo," *Nat. Methods,* vol. 8, no. 4, pp. 319-325, 2011, doi: 10.1038/nmeth.1572.
[9] T. Gerfin and M. Grätzel, "Optical properties of tin-doped indium oxide determined by spectroscopic ellipsometry," *JAP,* vol. 79, no. 3, pp. 1722-1729, 1996, doi: 10.1063/1.360960.
[10] C. Calahoo and L. Wondraczek, "Ionic glasses: Structure, properties and classification," *J. Non-Cryst. Solids: X,* p. 100054, 2020, doi: 10.1016/j.nocx.2020.100054.
[11] A. Levasseur, J.-C. Brethous, J.-M. Réau, and P. Hagenmuller, "Etude comparee de la conductivite ionique du lithium dans les halogenoborates vitreux," *Mater. Res. Bull.,* vol. 14, no. 7, pp. 921-927, 1979, doi: 10.1016/0025-5408(79)90158-2.
[12] H. Jain, H. Downing, and N. Peterson, "The mixed alkali effect in lithium-sodium borate glasses," *J. Non·Cryst. Solids,* vol. 64, no. 3, pp. 335-349, 1984, doi: 10.1016/0022-3093(84)90187-X.
[13] S. W. Martin, "Ionic conduction in phosphate glasses," *J. Am. Ceram. Soc.,* vol. 74, no. 8, pp. 1767-1784, 1991, doi: 10.1111/j.1151-2916.1991.tb07788.x.
[14] B. Poletto Rodrigues, R. Limbach, G. Buzatto de Souza, H. Ebendorff-Heidepriem, and L. Wondraczek, "Correlation between ionic mobility and plastic flow events in NaPO3-NaCl-Na2SO4 glasses," *Front. Mater.,* vol. 6, p. 128, 2019, doi: 10.3389/fmats.2019.00128.
[15] P. C. Schultz and M. S. Mizzoni, "Anionic Conductivity in Halogen-Containing Lead Silicate Glasses," *J. Am. Ceram. Soc.,* vol. 56, no. 2, pp. 65-68, 1973, doi: 10.1111/j.1151-2916.1973.tb12359.x.
[16] A. Abd El-Mongy, "Effect of halogen on the structure and ionic conductivity of silicate glasses," *Phys. Status Solidi A,* vol. 144, no. 1, pp. 17-22, 1994, doi: 10.1002/pssa.2211440103.
[17] K. Tanaka, T. Yoko, K. Kamiya, H. Yamada, and S. Sakka, "Properties of oxybromide tellurite glasses in the system LiBr-Li2O-TeO2," *J. Non·Cryst. Solids,* vol. 135, no. 2-3, pp. 211-218, 1991, doi: 10.1016/0022-3093(91)90422-3.
[18] H. Ebendorff-Heidepriem, Y. Ruan, H. Ji, A. D. Greentree, B. C. Gibson, and T. M. Monro, "Nanodiamond in tellurite glass Part I: origin of loss in nanodiamond-doped glass," *Opt. Mater. Express,* vol. 4, no. 12, pp. 2608-2620, 2014, doi: 10.1364/OME.4.002608.
[19] N. Tagiara, D. Palles, E. Simandiras, V. Psycharis, A. Kyritsis, and E. Kamitsos, "Synthesis, thermal and structural properties of pure TeO2 glass and zinc-tellurite glasses," *J. Non·Cryst. Solids,* vol. 457, pp. 116-125, 2017, doi: 10.1016/j.jnoncrysol.2016.11.033.
[20] A. Pan and A. Ghosh, "Activation energy and conductivity relaxation of sodium tellurite glasses," *PhRvB,* vol. 59, no. 2, p. 899, 1999, doi: 10.1103/PhysRevB.59.899.
[21] K. B. Kavaklıoğlu, S. Aydin, M. Çelikbilek, and A. E. Ersundu, "The TeO2-Na2O System: Thermal Behavior, Structural Properties, and Phase Equilibria," *Int. J. Appl. Glass Sci.,* vol. 6, no. 4, pp. 406-418, 2015, doi: 10.1111/ijag.12103.

[22] S. K. Bondarenko, L. V. Udovichenko, A. I. Mitichkin, N. N. Kosinov, and I. V. Khromaya, "Optical and Scintillation Properties of NaI(Tl) Crystals," *JApSp,* vol. 69, no. 6, 2002, doi: 10.1023/A:1022422823022.
[23] Y. Wei, J. Zhao, S. Fuhrmann, R. Sajzew, L. Wondraczek, and H. Ebendorff-Heidepriem, "Controlled formation of gold nanoparticles with tunable plasmonic properties in tellurite glass," *Light Sci Appl,* vol. 12, no. 1, p. 293, 2023, doi: 10.1038/s41377-023-01324-x.
[24] H. Ebendorff-Heidepriem, K. Kuan, M. R. Oermann, K. Knight, and T. M. Monro, "Extruded tellurite glass and fibers with low OH content for mid-infrared applications," *Opt. Mater. Express,* vol. 2, no. 4, pp. 432-442, 2012, doi: 10.1364/OME.2.000432.
[25] T. Rouxel, "Elastic properties and short-to medium-range order in glasses," *J. Am. Ceram. Soc.,* vol. 90, no. 10, pp. 3019-3039, 2007, doi: 10.1111/j.1551-2916.2007.01945.x.
[26] R. D. Shannon, "Shannon, Revised effective ionic radii and systematic studies of interatomic distances in halides and chalcogenides," *Acta crystallographica section A: crystal physics, diffraction, theoretical and general crystallography,* vol. 32, no. 5, pp. 751-767, 1976, doi: 10.1107/S0567739476001551.
[27] A. Kalampounias, S. Yannopoulos, and G. Papatheodorou, "Vibrational modes of sodium–tellurite glasses: Local structure and Boson peak changes," *J. Phys. Chem. Solids,* vol. 68, no. 5-6, pp. 1035-1039, 2007, doi: 10.1016/j.jpcs.2007.01.048.
[28] M. F. Ando *et al.*, "Boson peak, heterogeneity and intermediate-range order in binary SiO2-Al2O3 glasses," *Sci. Rep.,* vol. 8, no. 1, pp. 1-14, 2018, doi: 10.1038/s41598-018-23574-1.
[29] A. Šantić, A. Moguš-Milanković, K. Furić, M. Rajić-Linarić, C. S. Ray, and D. E. Day, "Structural properties and crystallization of sodium tellurite glasses," *Croat. Chem. Acta,* vol. 81, no. 4, pp. 559-567, 2008.
[30] T. Sekiya, N. Mochida, A. Ohtsuka, and M. Tonokawa, "Raman spectra of MO1/2TeO2 (M= Li, Na, K, Rb, Cs and Tl) glasses," *J. Non·Cryst. Solids,* vol. 144, pp. 128-144, 1992, doi: 10.1016/S0022-3093(05)80393-X.
[31] N. Tagiara, E. Moayedi, A. Kyritsis, L. Wondraczek, and E. Kamitsos, "Short-range structure, thermal and elastic properties of binary and ternary tellurite glasses," *J. Phys. Chem. B,* vol. 123, no. 37, pp. 7905-7918, 2019, doi: 10.1021/acs.jpcb.9b04617.
[32] T. Sekiya, N. Mochida, A. Ohtsuka, and M. Tonokawa, "Normal vibrations of two polymorphic forms of TeO2 crystals and assignments of Raman peaks of pure TeO2 glass," *J. Ceram. Soc. Jpn.,* vol. 97, no. 1132, pp. 1435-1440, 1989, doi: 10.2109/jcersj.97.1435.
[33] S. Manning, H. Ebendorff-Heidepriem, and T. M. Monro, "Ternary tellurite glasses for the fabrication of nonlinear optical fibres," *Opt. Mater. Express,* vol. 2, no. 2, pp. 140-152, 2012, doi: 10.1364/OME.2.000140.
[34] M. Jesuit *et al.*, "Analysis of Physical and Structural Properties of Alkali Oxide–Modified Tellurite Glasses," *J. Undergrad. Rep. Phys.,* vol. 30, no. 1, p. 100003, 2020, doi: 10.1063/10.0002043.
[35] N. A. Wójcik *et al.*, "The influence of Be addition on the structure and thermal properties of alkali-silicate glasses," *J. Non·Cryst. Solids,* vol. 521, p. 119532, 2019, doi: 10.1016/j.jnoncrysol.2019.119532.
[36] A. G. Kalampounias, "Low-frequency Raman scattering in alkali tellurite glasses," *Bull. Mater. Sci.,* vol. 31, no. 5, pp. 781-785, 2008, doi: 10.1007/s12034-008-0124-z.
[37] M. Baggioli and A. Zaccone, "Universal origin of boson peak vibrational anomalies in ordered crystals and in amorphous materials," *Phys. Rev. Lett.,* vol. 122, no. 14, p. 145501, 2019, doi: 10.1103/PhysRevLett.122.145501.
[38] V. K. Malinovsky and A. P. Sokolov, "The nature of boson peak in Raman scattering in glasses," *Solid State Commun.,* vol. 57, no. 9, pp. 757-761, 1986, doi: 10.1016/0038-1098(86)90854-9.
[39] H. Shintani and H. Tanaka, "Universal link between the boson peak and transverse phonons in glass," *Nat. Mater.,* vol. 7, no. 11, pp. 870-877, 2008, doi: 10.1038/nmat2293.

[40] O. V. Shishkin, A. Pelmenschikov, D. M. Hovorun, and J. Leszczynski, "Theoretical analysis of low-lying vibrational modes of free canonical 2-deoxyribonucleosides," *ChPh,* vol. 260, no. 3, pp. 317-325, 2000, doi: 10.1016/S0301-0104(00)00251-2.

[41] S. Balaji, K. Biswas, A. D. Sontakke, G. Gupta, D. Ghosh, and K. Annapurna, "Al2O3 influence on structural, elastic, thermal properties of Yb3+ doped Ba–La-tellurite glass: Evidence of reduction in self-radiation trapping at 1 μm emission," *Spectrochim. Acta A Mol. Biomol. Spectrosc.,* vol. 133, pp. 318-325, 2014, doi: 10.1016/j.saa.2014.04.113.

[42] C. D. Bordon, E. S. Magalhaes, D. M. da Silva, L. R. Kassab, and C. B. de Araújo, "Influence of Al2O3 on the photoluminescence and optical gain performance of Nd3+ doped germanate and tellurite glasses," *Opt. Mater.,* vol. 109, p. 110342, 2020, doi: 10.1016/j.optmat.2020.110342.

[43] P. Wang, C. Wang, W. Li, M. Lu, and B. Peng, "Effects of Al2O3 on the thermal stability, glass configuration of Yb3+-doped TeO2–K2O–ZnO–Al2O3 based tellurite laser glasses," *J. Non·Cryst. Solids,* vol. 359, pp. 5-8, 2013, doi: 10.1016/j.jnoncrysol.2012.09.031.

[44] S. Sakida, S. Hayakawa, and T. Yoko, "125Te, 27Al, and 71Ga NMR study of M2O3–TeO2 (M= Al and Ga) glasses," *J. Am. Ceram. Soc.,* vol. 84, no. 4, pp. 836-842, 2001, doi: 10.1111/j.1151-2916.2001.tb00749.x.

[45] T. Allison, "JANAF thermochemical tables, NIST standard reference database," vol. 13, p. 1453, 1996, doi: 10.18434/T42S31.

[46] J. J. Reed, "The NBS Tables of Chemical Thermodynamic Properties: Selected Values for Inorganic and C1 and C2 Organic Substances in SI Units"," *J. Res. Natl. Inst. Stand. Technol.,* vol. 125, 2020, doi: 10.18434/M32124.